PCCP

View Online
Dynamic Article Links

Cite this: *Phys. Chem. Chem. Phys.*, 2011, **13**, 11985–11997

www.rsc.org/pccp

PAPER

Fluorescence quantum yield and photochemistry of bacteriophytochrome constructs†

K. C. Toh,‡[a] Emina A. Stojković,§[b] Ivo H. M. van Stokkum,[a] Keith Moffat[bc] and John T. M. Kennis*[a]

Received 6th January 2011, Accepted 5th May 2011
DOI: 10.1039/c1cp00050k

Bacteriophytochromes (Bphs) are red-light photoreceptor proteins with a photosensory core that consists of three distinct domains, PAS, GAF and PHY, and covalently binds biliverdin (BV) to a conserved cysteine in the PAS domain. In a recent development, PAS–GAF variants were engineered for use as a near-infrared fluorescent marker in mammalian tissues (Tsien and co-workers, *Science,* 2009, **324**, 804–807). Here, we report the fluorescence quantum yield and photochemistry of two highly-related Bphs from *Rps. palustris*, RpBphP2 (P2) and RpBphP3 (P3) with distinct photoconversion and fluorescence properties. We applied ultrafast spectroscopy to wild type P3 and P2 PAS–GAF proteins and their P3 D216A, Y272F and P2 D202A PAS–GAF–PHY mutant proteins. In these mutants hydrogen-bond interactions between a conserved aspartate (Asp) which connects the BV chromophore with the PHY domains are disrupted. The excited-state lifetime of the truncated P3 and P2 PAS–GAF proteins was significantly longer than in their PAS–GAF–PHY counterparts that constitute the full photosensory core. Mutation of the conserved Asp to Ala in the PAS–GAF–PHY protein had a similar but larger effect. The fluorescence quantum yields of the P3 D216A and Y272F mutants were 0.066, higher than that of wild type P3 (0.043) and similar to the engineered Bph of Tsien and co-workers. We conclude that elimination of a key hydrogen-bond interaction between Asp and a conserved Arg in the PHY domain is responsible for the excited-state lifetime increase in all Bph variants studied here. H/D exchange resulted in a 1.4–1.7 fold increase of excited-state lifetime. The results support a reaction model in which deactivation of the BV chromophore proceeds *via* excited-state proton transfer from the BV pyrrole nitrogens to the backbone of the conserved Asp or to a bound water. This work may aid in rational structure- and mechanism-based conversion of constructs based on P3 and other BPhs into efficient near-IR, deep tissue, fluorescent markers.

Introduction

Phytochromes are red-light sensing proteins found in plants, bacteria, cyanobacteria and fungi that act as photochromic switches activated by distinct wavelengths in the red or far red regions.[1–8] Their light-sensing module comprises PAS, GAF and PHY domains and covalently binds a linear tetrapyrrole, phycochromobilin (PΦB) in plant phytochromes, phycocyanobilin (PCB) in cyanobacterial phytochromes, and biliverdin (BV) in bacteriophytochromes (BPh). They exist as dimers in which interfaces between the monomers are formed both by the N-terminal photosensory core and the C-terminal kinase domain.[9] In the dark, most phytochromes adopt a red-absorbing state known as Pr and upon light absorption convert to a far-red absorbing state known as Pfr. The light activation mechanism involves an isomerization process about the C15═C16 double bond of the linear tetrapyrrole, changing its configuration from 15*Za* to 15*Ea*.[10–12] Light-induced *Z*/*E* isomerization of the tetrapyrrole takes place on a timescale of tens to hundreds of ps.[13–18] The reaction then proceeds through several intermediate, spectroscopically-distinct states such as Lumi-R before the Pfr state is established.[19–22]

The recent determination of crystal structures of various BPhs, the cyanobacterial phytochrome Cph1 and the NMR structure of the single domain, GAF-only cyanobacterial

[a] *Biophysics Section, Department of Physics and Astronomy, VU University, De Boelelaan 1081, 1081HV Amsterdam, The Netherlands. E-mail: j.t.m.kennis@vu.nl*
[b] *Department of Biochemistry and Molecular Biology, The University of Chicago, USA*
[c] *Institute for Biophysical Dynamics, The University of Chicago, USA*
† Electronic supplementary information (ESI) available. See DOI: 10.1039/c1cp00050k
‡ Current address: Division of Molecular Biosciences, Imperial College, London, UK.
§ Current address: Department of Biology, Northeastern Illinois University, Chicago, IL, USA.

SyB[23] has explored the light-activated function of phytochromes.[10,11,24–26] BPhs bind BV through a covalent thioether linkage to the PAS domain. BV is largely engulfed by the GAF domain, which provides most of the hydrogen bonding, steric and hydrophobic interactions that secure the chromophore in position.[10,24,26,27] The pyrrole rings form an intricate hydrogen-bond network in which a conserved Asp, a conserved His and a water molecule interact with the pyrrole nitrogens (Fig. 1). The PHY domain extends the PAS–GAF core to tune spectral properties and facilitate physiologically functional photochemistry. Crystal structures of the complete photosensory core module comprising the PAS–GAF–PHY domains are available only for Cph1 in the Pr state and *Pseudomonas* PaBphP in the Pfr state.[10,28] For P3 and *Deinococcus* Bph (DrBphP), structures of only the PAS–GAF domains are known.[24–26] The PHY domain engages the chromophore pocket through hydrogen bonding with the conserved Asp, and seals off the chromophore from contact from the solvent. Deletion of the PHY domain affects the photochemistry and impairs Pfr formation.[26,29]

In an important recent development, the PAS–GAF protein from DrBphP was engineered by Shu, Tsien and co-workers for use as a fluorescent marker in mammalian tissues.[30] Fluorescent phytochromes were first reported by Fischer and

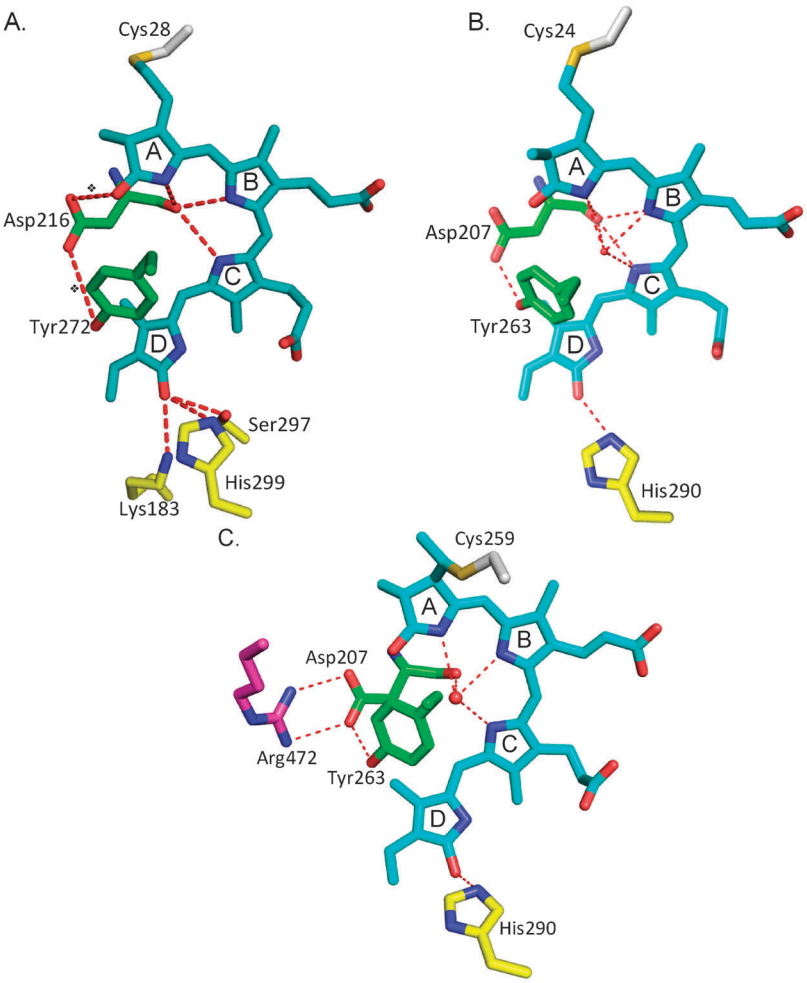


```
                183          216   272                    297
RpBphP3   -KVYQFA-HFPSSDIPAQ—YMVNMGMHAAMSISIVRDNRLWGMISCHNL-
RpBphP2   -MIYRFA-HFPASDIPAQ—YMRNIGMHGTMSISILRGERLWGLIACHHR-
DrBphP    -MAYRFR-RFPASDIPAQ—YLRNMGVGSSLSVSVVVGGQLWGLIACHHQ-
AtBphP1   -LIYDFG-RFPAGDIPPQ—YMRNMGTAASMSVSIVVNGALWGLIACHHA-
PaBphP    -MLYKFA-RYPASDIPAQ—YLTNMGVRASMSISIVVGGKLWGLFSCHHM-
Cph1      -MLYRFD-HYPESDIPQP—YLKNMGVGASLTISLIKDGHLWGLIACHHQ-
```

Fig. 1 (A) The BV binding site in the X-ray structure (Protein Data Bank code 2OOL) of *Rhodopseudomonas palustris* P3; (B) the BV binding site in the X-ray structure (1ZTU) of *Deincococcus radiodurans* DrBphP; (C) the BV binding site in the X-ray structure (2VEA) of the Cph1 full length construct in the Pr ground state. Asp-207 of the PASDIP motif in the GAF domain forms together with its main chain an extensive hydrogen bonding network with the chromophore and Arg-472 in the PRSXF motif of the PHY domain; lower panel: partial protein sequence alignment of bacteriophytochromes P3 and P2 from *Rhodopseudomonas palustris*, DrBphP from *Deinoccocus radiodurans*, AtBphP1 from *Agrobacterium tumafeciens*, PaBphP from *Pseudomonas aeruginosa* and cyanobacterial phytochrome Cph1 from *Synechocystis sp. pcc 6803*. Numerical values indicate positions of amino acids in P3 primary sequence.

Lagarias[31] and Vierstra and co-workers.[32] DrBphP fluoresces in the near-IR at ~720 nm, a wavelength substantially longer than that emitted by GFP-derived fluorescent proteins. Longer-wavelength fluorescence is less prone to scattering and therefore can penetrate more deeply into tissue. Shu *et al.*[30] engineered the PAS–GAF chromophore binding domain of DrBphP to yield a monomeric protein with a fluorescence quantum yield of 0.07, and explored a series of mutations around BV ring D and the dimerization surface. Recent work by Zhao and co-workers explored alternative routes to produce fluorescent phytochromes.[33] Since BV is a naturally occurring cofactor in mammalian tissue that covalently binds in an uncatalyzed reaction to a conserved cysteine in the PAS domain, BPhs can readily be genetically encoded and assembled *in vivo*. BPh photochemistry is thus of considerable significance for biomedical research and technology. However, Bph fluorescence properties and in particular the fluorescence quantum yield need substantial improvement for routine applications as a fluorescence marker. This led us to explore other Bphs and domain constructs which might offer improved fluorescence properties.

BPhs RpBphP2 (P2) and RpBphP3 (P3) from *Rhodopseudomonas palustris* are examples of classical and non-classical phytochromes respectively that have a common ground state (Pr) but different photoactivated states. Upon illumination, P2 forms the classical Pfr state. P3 is unique with respect to classical phytochromes: it forms a near-red light absorbing state at 645 nm denoted Pnr[22] and in particular, its ring D is restrained by three hydrogen bonds from His, Ser and Lys side chains to its carbonyl group (Fig. 1A).[26] In classical Bphs, only one hydrogen bond from His stabilizes ring D (Fig. 1B).[24,25] In our recent femtosecond time-resolved absorption studies on the complete, three-domain, PAS–GAF–PHY photosensory core modules of P2 and P3, we showed that the excited state lifetimes and the spectra of P3 differ substantially from those of P2 and other classical Bphs.[13,34] Strikingly, the BV excited state of P3 decayed with a monoexponential time constant of 330 ps, significantly longer than that observed in P2 and other phytochromes. We related these differences to the number and strength of the hydrogen bonds between the protein and ring D.[34] We determined that the presence of two additional polar residues, lysine and serine located in the immediate vicinity of ring D, lowers the quantum yield for Lumi-R formation and increases the excited-state lifetime of BV. Excited-state decay predominantly proceeds through an excited-state proton transfer reaction (ESPT) from the pyrrole nitrogens to a conserved Asp or to bound water. Altogether, the fluorescence quantum yield of P3 is significantly higher than that of classical Bph. With detailed knowledge of its structure and excited-state dynamics, P3 forms an attractive starting material on which to base a fluorescent probe.

Under the assumption that the Pr states of the PAS–GAF–PHY constructs of P2 and P3 are structurally similar to that of Cph1 (whose X-ray structure from Protein Data Bank entry 2VEA is shown in Fig. 1), the BV chromophore forms an intricate hydrogen-bond network with the main-chain carbonyl of conserved Asp from the Proline-Alanine-Serine-Aspartate-Isoleucine-Proline (PASDIP) sequence motif and a bound water at its pyrrole nitrogens. In turn, the Asp side chain forms double hydrogen bonds with a conserved Arg from the PRXSF motif in the PHY domain. Thus, Asp bridges BV with the PHY domain through extensive hydrogen bonding.

Here, we explore the consequences of the absence of the PHY domain for photochemistry and the quantum yield for fluorescence. We experimentally address the impact of the hydrogen-bond network on these factors through an ultrafast transient absorption and time-resolved fluorescence study of truncated P2 and P3 variants that comprise only the PAS and GAF domains, and of PAS–GAF–PHY constructs where the conserved Asp from the PASDIP motif is replaced by Ala. These Bph variants exhibit a further increase of the fluorescence quantum yield with respect to wild type PAS–GAF–PHY proteins. Importantly, none of these constructs form a canonical Pfr or Pnr state.[26] This work provides important clues for understanding the light activation mechanism of Bph that can be utilized for further development of Bph PAS–GAF proteins into an efficient near-infrared deep-tissue fluorescent probe by means of rational structure- and mechanism-based engineering.[13]

Materials and methods

Sample preparation

The detailed preparation of P2 and P3 PAS–GAF BPhs, the P2 PAS–GAF–PHY D202A mutant and the P3 PAS–GAF–PHY D216A mutant was described previously.[26] Proteins were dissolved in a 20 mM TRIS·HCl buffer at pH 8. For H/D exchange experiments, they were dissolved in D_2O buffer (20 mM TRIS·HCl, pD 8 at room temperature). H/D exchange was carried out by removing the H_2O buffer using an Amicon filter (30 kD) and an ultracentrifuge, and then adding the D_2O buffer to dilute the protein concentration. These procedures were repeated for at least 6 times to minimize the content of the H_2O buffer. The deuterated proteins were prepared at least 24 hours prior to the experiments. On the day of the experiments, the samples (in D_2O buffer) were further diluted by adding D_2O buffer.

Femtosecond transient absorption spectroscopy

Femtosecond transient absorption experiments were performed using the amplified Ti:sapphire-based laser setup described previously.[35] A seed pulse from a diode-pumped oscillator (Coherent Vitesse, 800 nm, 76.6 MHz, 50 fs) was amplified to 2.5 W by using a Nd:YLF high-power pump-laser (Coherent Evolution-20, 527 nm, 1 kHz). The Ti:Sapphire-based amplifier (Coherent Legend-USP) incorporates chirped pulse amplification and a stretcher/compressor combination to deliver sub-50 fs pulses, with a centre wavelength at 800 nm and a bandwidth of 30 nm (FWHM) at a repetition rate of 1 kHz. The beam was guided into an optical parametric amplification setup (Coherent OpeRA), which converts the pump laser output to a tunable pair of outputs: the signal (1150–1600 nm) and the idler (1600 nm–2630 nm). To generate a 680 nm pump beam, the signal at 1360 nm was frequency-doubled in a nonlinear crystal. A small fraction of the initial 800 nm beam was used to generate the white-light probe light using a sapphire crystal.

The protein solution was contained in a quartz flow cuvette with 2 mm path length. A diaphragm metering pump (STEPDOS 03S from KNF Neuberger, Inc.) was used to flow fresh sample to the cuvette from an external reservoir with 3–4 ml sample volume. Background illumination to photorevert the Bph sample to Pr was provided with an LED of center wavelength 750 nm (P2 D202A, P2 PAS–GAF and P3 PAS–GAF) or 650 nm (P3 D216A). Alternatively, a 2 mm quartz sample cuvette was attached to a high frequency shaker and used without flow, but retaining direct illumination by a 750 nm or 650 nm LED. The flow and shaking cuvette methods gave identical results. The sample had an absorbance of about 0.2–0.4 for a 2 mm sample thickness at the excitation wavelength. Both the pump light of 680 nm with energy of 200 nJ to 400 nJ (generated from the OPA-SFG) and the probe light are focused and overlapped at the sample in the cuvette. The probe light was focused on the entrance slit of a spectrograph, spectrally dispersed and projected on a 256 diode-array detector. The spectral resolution was 1.2 nm. A reference dataset using water was collected under identical experimental conditions and used to correct artifacts caused by cross-phase modulation near time zero arising from interaction between the probe and the pump pulses in the solvent and on the cuvette windows.

Time-resolved fluorescence spectroscopy

Time-resolved fluorescence measurements were carried out using the streak camera setup described earlier.[36,37] An integrated Ti-sapphire oscillator (Coherent Vitesse) produced pulses of 800 nm with 100 fs duration at 80 MHz repetition rate. This beam was directed into a regenerative amplifier (Coherent RegA) operating rate between 48 kHz to 128 kHz and then fed into an optical parametric amplifier (Coherent OPA) tunable between 470 and 720 nm. The pump light was focused on a 1 cm path length quartz cuvette placed on a magnetic stirrer. The sample (with an absorbance of 0.1) was excited by the 680 nm laser beam. Background illumination used a 750 nm or 650 nm LED to revert the light-activated sample to the ground state. Fluorescence emission from the sample was collected at right angles to the pump beam and focused into the slit and grating using an achromatic lens. A sheet polarizer was used to adjust the magic angle (54.7°, with respect to the polarization angle of the pump beam) of the collected emission. The dispersed light was converted to electrons at the photocathode and time-resolved by varying the voltage applied to sweep electrodes. A microchannel-plate (MCP) was used to amplify the photocathode signal and projected to a phosphor screen where it was visualized by a CCD camera.

Data analysis

The femtosecond transient absorption data were globally analyzed using a kinetic model consisting of sequentially interconverting, evolution-associated difference spectra (EADS), *i.e.* 1 → 2 → 3 → ... in which the arrows indicate successive mono-exponential decays of increasing time constant, which can be regarded as the lifetime of each EADS.[38] The first EADS corresponds to the time-zero difference spectrum. This procedure clearly visualizes the evolution of the (excited and intermediate) states of the system. In time-resolved fluorescence measurements, an independent exponential decay scheme (sum of exponentials) is applied which produces the decay associated spectra (DAS). It is important to note that a sequential analysis is mathematically equivalent to a parallel (sum-of-exponentials) analysis. The analysis program calculates both EADS and decay-associated difference spectra (DADS), and the time constants that follow from the analysis apply to both. Throughout the manuscript, the EADS are shown in the main text and the corresponding DADS are shown in ESI.† In general, the EADS may well reflect mixtures of molecular states such as may arise, for instance, from heterogeneous ground states or branching at any point in the molecular evolution.[13,39–44] The advantage of showing EADS over DADS is that the former are qualitatively and intuitively more easily interpreted in terms of which molecular species is present at what time. We stress that the sequential model used in this approach to data analysis should not *a priori* be taken literally. The combination of different time-resolved spectroscopy information such as the transient absorption and time-resolved fluorescence with close inspection of EADS, DADS and DAS is required to arrive at conclusions regarding the parallel, branched or sequential nature of the spectral evolution. A detailed account of the global analysis methodology is given in ESI.†

Fluorescence quantum yield experiments

Fluorescence quantum yield measurements were performed using a commercial fluorometer with right-angle detection geometry (Jobin-Yvon Fluorolog). Cy5 dissolved in water was used as a fluorescence quantum yield standard (Φ_F = 0.27).[45] The samples were contained in a cuvette with 1 cm pathlength in the excitation direction and 0.4 cm pathlength in the detection direction. The excitation wavelength was 645 nm. The absorbance of Bph and reference samples were adjusted to similar values at the excitation wavelength and the absorbance of Bph at the maximum of the Q band was less than 0.03 per cm pathlength. The excitation density was kept low to avoid photoconversion of the Bph samples; its absence was confirmed by the identity of absorbance spectra immediately before and after the fluorescence experiments. The fluorescence intensities were corrected for the number of absorbed photons. The fluorescence spectra were corrected for the wavelength sensitivity of the detection system and converted to an energy scale, thereby correcting the change in bandpass through the relation $I(\nu) = l^2 I(\lambda)$.[46] The fluorescence spectra were recorded and integrated up to 850 nm. All experiments were performed at room temperature.

Results

Fluorescence properties of bacteriophytochromes

Fig. 2 shows fluorescence emission spectra of P3 PAS–GAF–PHY (red line), the two-domain version of P3 PAS–GAF chromophore binding domain (CBD) (blue), the P3 PAS–GAF–PHY D216A mutant (cyan), the P3 PAS–GAF–PHY Y272F mutant (black) and the classical BPh P2 PAS–GAF–PHY (dark green). The spectra are scaled to the number of absorbed

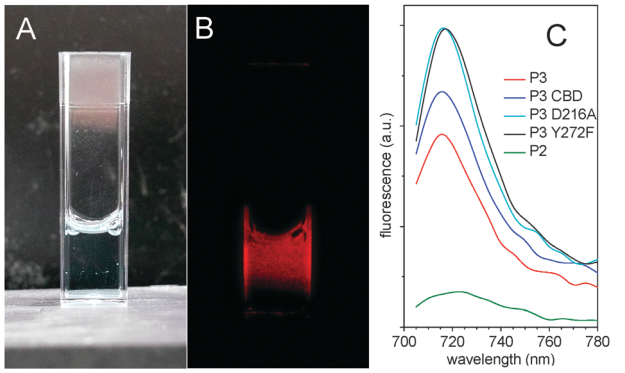

Fig. 2 Fluorescence properties of BPh. Photographs of the P3 Y272F mutant under (A) ambient light and (B) blue light at 405 nm, observed through a red-transmitting filter. (C) Fluorescence spectra of Bph samples indicated in the legend.

photons to enable their intensities to be directly compared. The fluorescence emission maxima of all samples are located near 715 nm, which indicates that the fluorescence originates from the BPh-bound BV chromophore. Their fluorescence quantum yields were determined to be 0.043 ± 0.005 (P3 PAS–GAF–PHY), 0.055 ± 0.005 (P3 PAS–GAF), 0.066 ± 0.005 (P3 PAS–GAF–PHY D216A) and 0.066 ± 0.005 (P3 PAS–GAF–PHY Y272F) In contrast, the classical BPh P2 (PAS–GAF–PHY) had a roughly five-fold lower fluorescence quantum yield of <0.01. Notably, the fluorescence quantum yield of the P3 PAS–GAF–PHY D216A and Y272F mutants is (within error margin) identical to that of the extensively engineered IFP1.4 PAS–GAF monomeric construct from *Deinococcus* BPh, namely 0.07.[30] Zhao and co-workers recently reported that a cyanobacteriochrome comprising an isolated GAF domain had a fluorescence quantum yield of 0.06.[33]

The photochemistry of wild type P3 PAS–GAF and the D216A and Y272F mutants of P3 PAS–GAF–PHY

The primary photochemistry of the unusual BPh P3 PAS–GAF was investigated by employing femtosecond time-resolved absorption spectroscopy. With excitation at 680 nm, the course of the time-resolved absorbance changes was monitored over the wavelength range from 550 to 780 nm. Global fitting of the data was applied using a kinetic scheme with sequentially interconverting species, where each species is represented by an evolution-associated difference spectrum (EADS). The EADS displays the difference spectrum of the photoexcited species of a particular lifetime with respect to the Pr ground state. Negative signals correspond to ground-state depletion (bleach) of the Pr state or to stimulated emission from the excited state to the ground state; positive signals denote absorption by the excited-state or product states. This procedure quantifies the spectral evolution. Five components were required for an adequate fit with lifetimes of 0.6, 4.9, 46, 408 ps and a non-decaying component. The resulting EADS are depicted in Fig. 3A and the decay-associated difference spectra (DADS) in Fig. S1A (ESI†). (The sub-ps component may have been affected by cross-phase modulation, coherent artifacts and saturation effects which render it difficult to interpret, and its spectra are therefore not shown.) Fig. 3B (black circles) shows a kinetic trace detected at 717 nm. The 4.9 ps component is associated with an overall red-shift of the transient absorption spectra, whose lifetime and spectral characteristics are very similar to those of the P3 PAS–GAF–PHY construct.[13] Importantly, this component does not represent excited-state decay: rather, we assign it to structural evolution on the excited state potential energy surface of the protein-bound BV. This can be clearly seen from the DADS in Fig. S1A (ESI†): the 4.9 ps DADS is largely conservative with a negative lobe at 690 nm and a positive lobe at 720 nm. A positive lobe can be interpreted as a decay of absorption, rise of bleach or stimulated emission; a negative lobe can be interpreted as a rise of absorption, decay of bleach or of stimulated emission. Ground-state bleach or stimulated emission should result in a relatively sharp feature near 700 nm, which is absent in the DADS. We therefore exclude the interpretation in which the 4.9 ps component represents BV excited-state decay. Instead, it represents a blue-shift of excited-state absorption or a red-shift of stimulated emission (or a combination of the two). Hence, it arises from dynamic processes in the BV excited state such as structural distortions.[13] Given the modest Huang–Rhys factor for vibronic coupling of BV and the excitation conditions in the main Q band, vibrational relaxation is unlikely to contribute to these processes.[47] As this paper primarily deals with excited-state decay processes in BPh, this component and similar ones described below for other P3 and P2 samples will not be further discussed.

The 46 ps component represents a minor spectral evolution: its DADS (Fig. S1A, green line, ESI†) primarily shows a small decay of ground state bleach, which indicates that this component represents a small fraction of nonemissive excited-state BPh that returns to the Pr ground state. In the P3 PAS–GAF–PHY construct an identical time constant was observed (45 ps) but with an entirely different spectral signature that involved a pronounced blue-shift of BV excited-state absorption.[13]

The next EADS has a lifetime of 408 ps. It shows a major ground state bleach at 708 nm, a smaller bleach band at 636 nm, and a pronounced excited-state absorption (ESA) around 725 nm. We assign this EADS to a structurally distorted BV in the excited state, in which the 408 ps time constant represents the excited-state lifetime. This interpretation is consistent with time-resolved fluorescence measurements (Fig. S2A and B, ESI†) which indicate a single exponential decay with a similar 382 ps time constant. These observations indicate that the excited-state lifetime of the P3 PAS–GAF construct is somewhat longer than that of P3 PAS–GAF–PHY with an excited-state lifetime of 330 ps.[13] The prolonged excited-state lifetime in P3 PAS–GAF induces a higher fluorescence quantum yield, when compared to classical phytochromes whose lifetimes range between 3 and 100 ps.[14–18,48]

The 408 ps EADS evolves to a component that does not decay on the timescale of the experiment (3 ns). It shows a ground state bleach at 702 nm and an induced absorption at around 731 nm. In phytochromes, such primary photoproducts are conventionally assigned to the Lumi-R intermediate state.[13,16–18] However, the spectral features of this particular

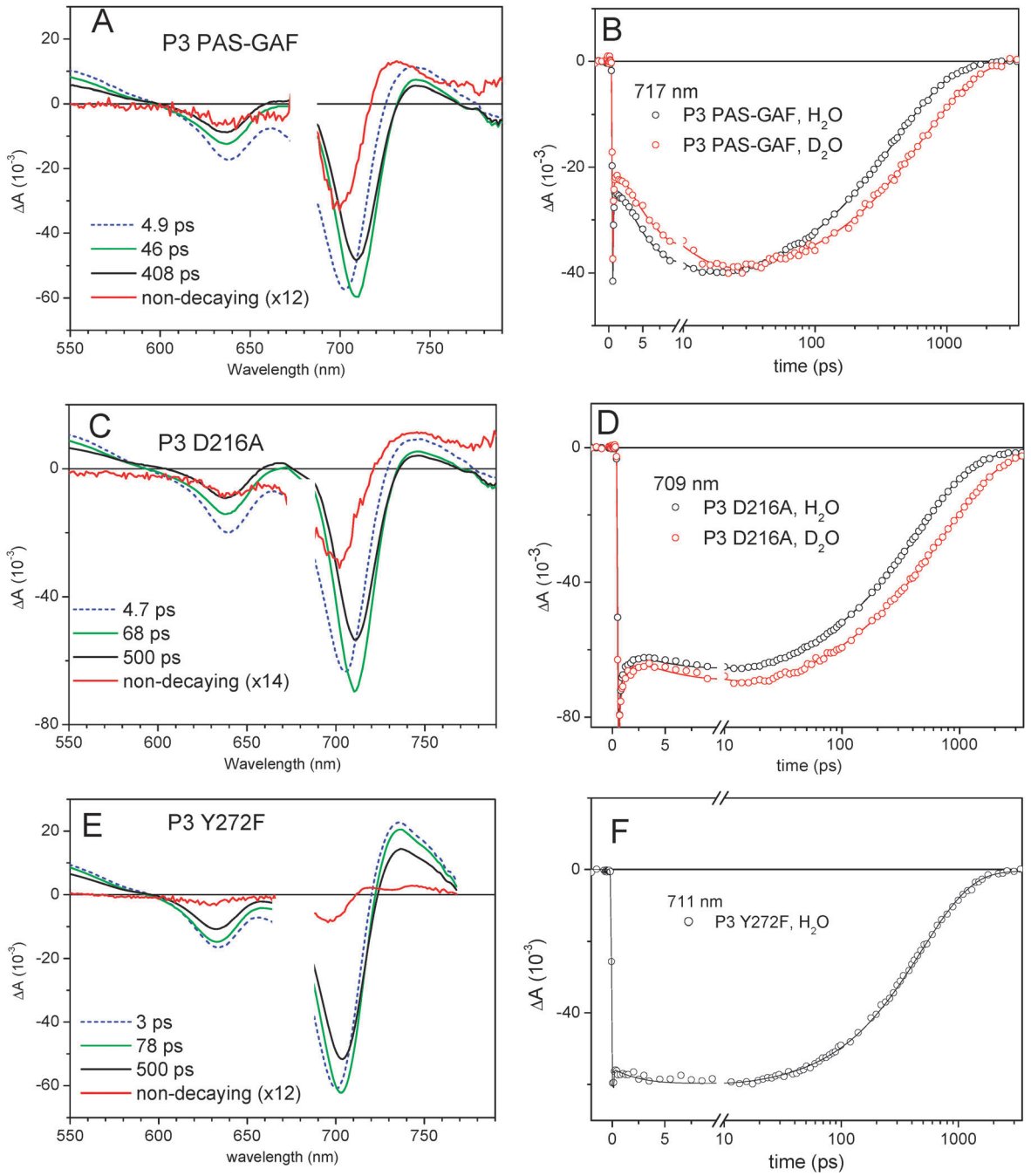

Fig. 3 Time-resolved spectroscopy of P3 PAS–GAF, the P3 PAS–GAF–PHY D216A mutant and the P3 PAS–GAF–PHY Y272F mutant. (A) Evolution-associated difference spectra (EADS) of P3 PAS–GAF; (B) kinetic traces of P3 PAS–GAF in H_2O (black circles) and D_2O (red circles); (C) EADS of the P3 D216A mutant; (D) kinetic traces of the P3 D216A mutant in H_2O (black circles) and D_2O (red circles); (E) EADS of the P3 Y272F mutant; (F) kinetic trace of the P3 Y272F mutant in H_2O.

photoproduct differ significantly from the Lumi-R species observed in the P3 PAS–GAF–PHY construct: the induced absorption band near 720 nm is broader and has a lower amplitude than in P3 PAS–GAF–PHY. It may have a different molecular origin, as discussed below. The amplitude of the primary photoproduct is very low with a remaining bleach of about 4% of the initial signal amplitude, as was also found in the P3 PAS–GAF–PHY protein (6%). With a fluorescence quantum yield of 0.06, this observation indicates that the vast majority ($\sim$0.9) of BV excited states deactivate nonradiatively to the Pr ground state.

The results on the D216A mutant of the PAS–GAF–PHY protein are similar overall to those on the P3 PAS–GAF construct. Global analysis indicated five components of 0.5, 4.7, 68, 500 ps and a non-decaying component. The EADS and DADS are shown in Fig. 3C and S1B, ESI†, respectively; Fig. 3D shows the kinetics at 709 nm. The EADS with lifetime of 500 ps, assigned to the BV excited state that decays in 500 ps

(green line), shows a significant longer time constant than that observed in P3 PAS–GAF–PHY (330 ps) and P3 PAS–GAF (408 ps). This observation is consistent with the steady-state fluorescence spectra shown in Fig. 2, in which the highest fluorescence intensity occurs for the P3 PAS–GAF–PHY D216A mutant.

The Y272F mutant is of special interest because along with D216A, it shows the highest fluorescence quantum yield (Fig. 2). In addition, it shows no photoproduct under steady-state illumination[26] which is a favorable property for fluorescence applications. Fig. 3E and S3 (ESI†) show the EADS and DADS, respectively, and the kinetics in Fig. 3F. The spectral evolution was similar to that of the P3 PAS–GAF and D216A proteins, with time constants of 3, 78, 500 ps and a nondecaying component. The 500 ps component represents BV excited-state decay, which is consistent with its relatively high fluorescence quantum yield. An important difference from the other BPh constructs reported here is that the amplitude of the primary photoproduct is significantly lower, roughly 4 times smaller than that for wild type P3, corresponding to a quantum yield of about 0.01. This low photoproduct quantum yield by itself does not explain the photochemical inactivity of Y272F under steady-state illumination, as photoreceptor proteins with similar photochemical quantum yields are known to fully convert to their lit state.[49] Hence, its photoproduct must be relatively short-lived.

The fluorescence quantum yields and excited-state lifetimes for the various P3 samples allow determination of the radiative lifetime of the BPh-bound BV chromophore. The fluorescence quantum yield Φ_F is related to fluorescence lifetime τ_F (*i.e.* the excited-state lifetime) and radiative lifetime τ_R through the relation $\tau_F = \Phi_F\tau_R$. With the experimentally observed fluorescence lifetimes and quantum yields for the P3 constructs, we obtain a radiative lifetime of about 7.5 ns for the BPh-bound BV chromophore. This number is significantly shorter than early reports for phytochrome-bound PΦB in the literature, which range from 14 ns to 20 ns.[50,51] However, these lifetimes were based on extinction coefficients ε that are now known to be incorrect. BPh has an extinction coefficient at its absorbance maximum in Pr of about 90 000 M^{-1} cm^{-1}.[5,30] A Strickler–Berg analysis of plant phytochrome A (PhyA) indicated a radiative lifetime of 5 ns, under the assumption that ε = 110 000 M^{-1} cm^{-1} at the absorbance maximum,[17] which reasonably agrees with our findings. (Note that ε = 121 000 M^{-1} cm^{-1} was reported by Lagarias and co-workers for plant phytochrome.)[52] In allophycocyanin (APC), the well-known fluorescence marker which binds PCB, a fluorescence quantum yield of 0.68[53] and a fluorescence lifetime of 4 ns[54] were reported, which implies a similar radiative lifetime of 5.9 ns.

The photochemistry of wild type P2 PAS–GAF and the D202A mutant of P2 PAS–GAF–PHY

To assess the influence of the PHY domain on the photochemistry of a classical BPh that exhibits Pr-Pfr photoconversion, we performed femtosecond time-resolved absorption spectroscopy studies on the P2 PAS–GAF construct. The structure of this construct is not yet known but is likely to be similar to the DrBphP protein, for which the high resolution X-ray structure[24,25] formed the basis for engineering by Shu *et al.*[30] as a fluorescent probe. Global analysis indicated that five components were required to fit the data, with time constants of 0.2, 4.4, 76, 284 ps and a non-decaying component. The EADS are shown in Fig. 4A and the DADS in Fig. S1D (ESI†). The sub-ps component is not shown. Fig. 4B shows the kinetics at 717 nm. As for P3, the 4.4 ps component is related to relaxation processes in the BV excited state. The EADS with a lifetime of 76 ps (black solid line) shows a ground state bleach/stimulated emission band at 716 nm, a stimulated emission shoulder at ~750 nm, a small bleach band at 648 nm and an excited-state absorption between 650 nm–700 nm. This EADS represents the structurally distorted excited state of BV[13] and evolves in 76 ps to the next EADS (red solid line) that has a lifetime of 284 ps. This EADS has an overall reduced amplitude in ground-state bleach, stimulated emission and excited-state absorption. This phenomenon is similar to the observation in the P2 PAS–GAF–PHY full length construct.[13] We assign the 284 ps EADS to a mixture of the BV excited state and the primary photoproduct; this mixture evolves in 284 ps to the primary photoproduct. All spectral signatures from the BV excited state are lost, with the remaining ground-state bleach at 701 nm, a minor bleach at 640 nm and an induced absorption at ~731 nm. The biexponential photoproduct formation from the BV excited state is also evident in the similar shapes of the 76 and 284 ps DADS in Fig. S1D (ESI†).

Fig. S2C and D (ESI†) shows the result of time-resolved fluorescence experiments performed on P2 PAS–GAF. The fluorescence lifetimes, 77 and 257 ps, are essentially identical to those observed with transient absorption. Thus, deletion of the PHY domain results in longer excited state lifetimes than in P2 PAS–GAF–PHY, where lifetimes of 43 and 170 ps were reported.[13]

To assess the role of the conserved Asp in the primary photochemistry of P2, we performed a femtosecond time-resolved absorption study on the D202A mutant of the PAS–GAF–PHY construct. Five components were required to fit the data, with time constants of 0.2, 4.4, 71, 383 ps, and a non-decaying component. Fig. 4C shows the EADS that result from a global analysis of the time-resolved experiments. The kinetics at 720 nm is shown in Fig. 4D and the DADS in Fig. S1E (ESI†). The 4.1 ps component is similar to that observed in the P2 PAS–GAF and PAS–GAF–PHY proteins. The 71 ps component represents a minor evolution and mainly involves decay of stimulated emission (Fig. S1D, ESI†). The 383 ps EADS (black solid line) represents BV excited-state decay. We conclude from these experiments that BV excited-state decay is almost single exponential at 383 ps, in stark contrast with wild type P2 where a biexponential decay was observed.[13]

H/D exchange effects

In our previous work, we observed significant H/D exchange effects on the excited-state dynamics of the P3 and P2 PAS–GAF–PHY proteins.[13] Here we show similar H/D exchange effects for their truncated PAS–GAF variants, as

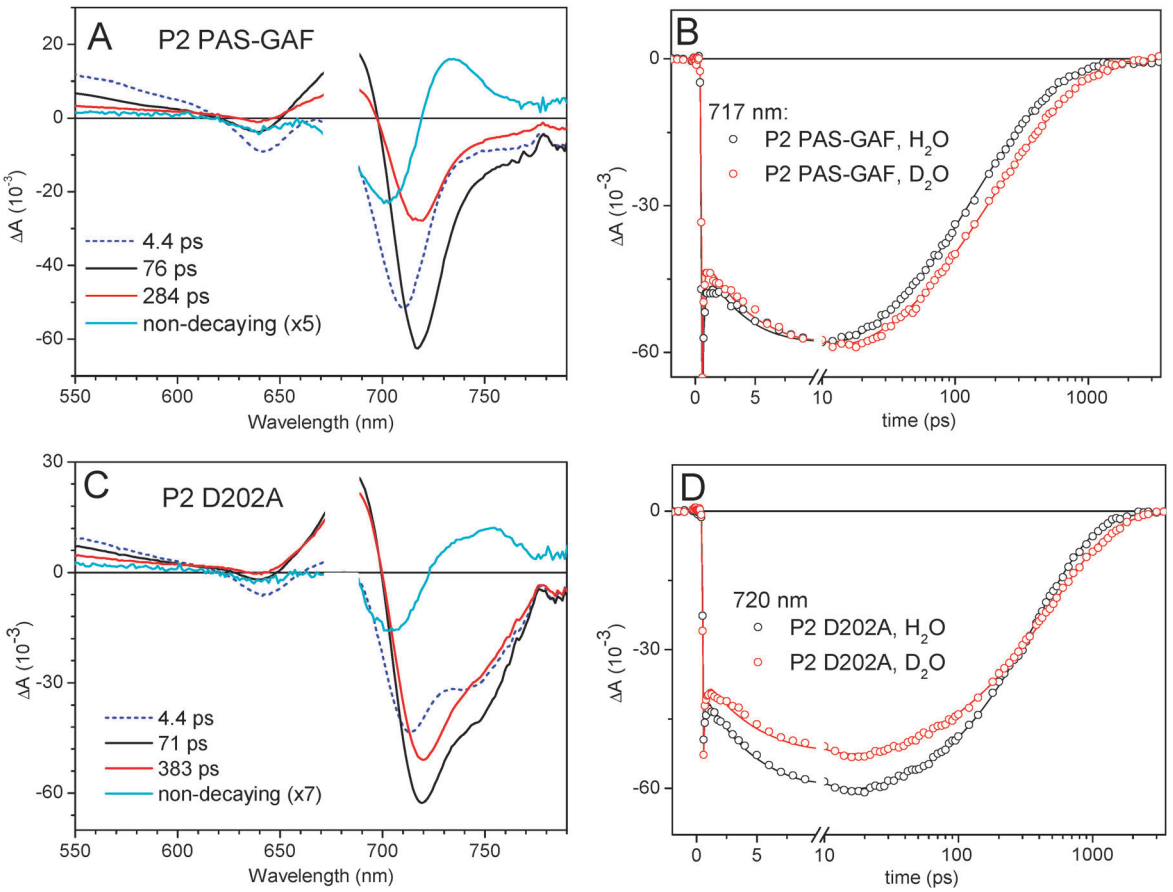

Fig. 4 Time-resolved spectroscopy of P2 PAS–GAF and the P2 PAS–GAF–PHY D202A mutant (A) evolution-associated difference spectra (EADS) of P2 PAS–GAF; (B) kinetic traces of P2 PAS–GAF in H_2O (black circles) and D_2O (red circles); (C) EADS of the P2 D202A mutant (D) kinetic traces of the P2 D202A mutant in H_2O (black circles) and D_2O (red circles);

observed in P3 PAS–GAF (Fig. 3B and Fig. S2B, ESI†, KIE 1.6) and P2 PAS–GAF (Fig. 4B and Fig. S2D ESI†, KIE $\approx$1.5 on the slow component). Likewise, the Asp to Ala mutants of P3 and P2 PAS–GAF–PHY show similar H/D exchange effects: the P3 PAS–GAF–PHY D216A mutant exhibits a KIE of 1.7 on its 500 ps excited-state lifetime, while the P2 PAS–GAF–PHY D202A mutant shows a KIE of 1.4 for its 383 ps excited-state lifetime. We conclude that in these BPh variants, excited-state deactivation to Pr is rate-limited by a proton transfer process similar to that observed in their wild type PAS–GAF–PHY constructs.

Discussion

ESPT affects the BV excited-state lifetime in bacteriophytochrome

Here and in our previous work we observed a significant kinetic isotope effect on the BV excited-state lifetime of BPh. We argued that the moderate KIE of $\sim$1.4 corresponds to a proton transfer reaction in the fully adiabatic limit, reflecting strong hydrogen-bond interactions between donor and acceptor groups and shallow barriers where the dominating effect of the KIE is reflected in isotope-dependent splitting in the crossing region of the potential surfaces in question.[13,55] Inspection of the BPh X-ray structure[26] indicated that an ESPT reaction at the pyrrole nitrogens constitutes the most likely explanation for the experimental observations. Note that all four pyrrole nitrogens are protonated in both the Pr and the Pfr states.[11,19,56,57] Fig. 5 schematically shows the proposed ESPT process. For clarity, Lumi-R formation was omitted from this figure. Note that ESPT may take place from either ring A, B or C.[13] Quantum chemical calculations on the PCB model chromophore indicate that rings B and C are the most acidic in the excited state,[58] which identifies these rings as the most likely proton donors.

Early work by Falk and co-workers suggested that in bilin pigments in solution, proton transfer at the pyrrole rings competes with Z/E isomerization,[59] which supports our reaction model. Quantum chemical studies of the PCB chromophore in solution indicated that ESPT processes significantly contributed to the excited-state dynamics.[60] Further support is provided by recent work on Agp1 variants with locked chromophores, which showed that processes additional to ring D motion can deactivate the BV excited state.[61] In addition, recent computational studies suggest that reduced accessibility to conformations geared to excited state proton transfer may be responsible for the increased fluorescence of engineered BPh.[62]

In general, moderate KIEs such as observed here may also correspond to solvent motions affected by the H/D exchange

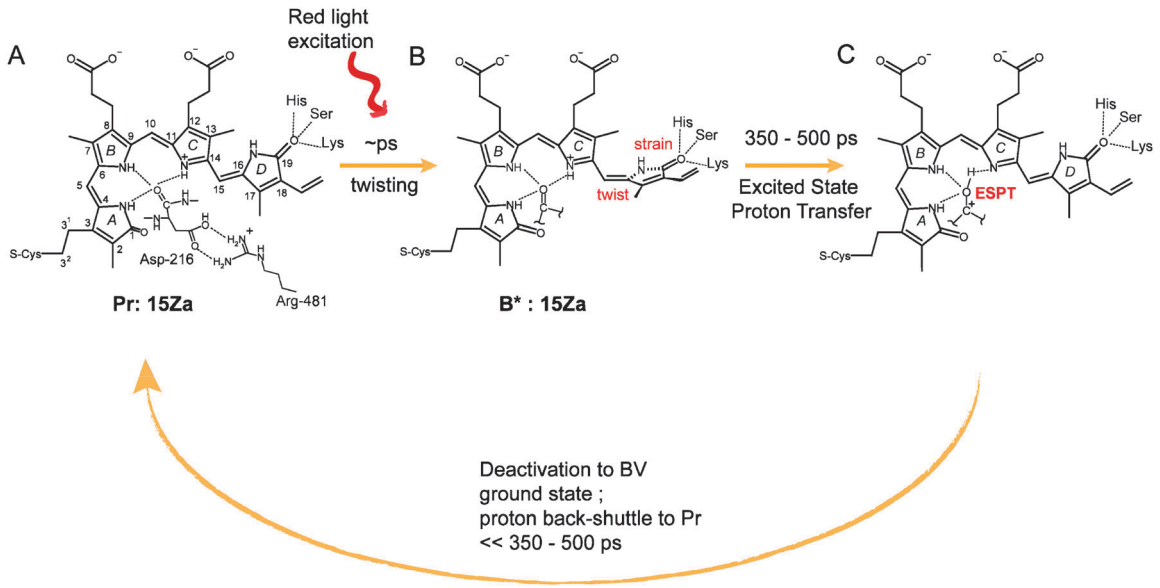

Fig. 5 Reaction scheme that accounts for BV excited-state deactivation in P3 through excited-state proton transfer, adapted from ref. 13. Panel (A) shows two hydrogen-bonds between Asp-216 in the GAF domain and Arg-481 in the PHY domain, as modeled on the basis of the Cph1 structure.[28] Note that this figure only considers the deactivation process to the Pr ground state; for a description of the full photochemistry see ref. 13.

that are somehow coupled to the reaction in question, rather than to an actual proton transfer event. However, in BPh the KIE acts on an excited-state deactivation process, which must be coupled to changes in the BV π-electron system. The latter is insensitive to the aqueous solvent. Likewise, a hydrogen-bond rearrangement between BV and apoprotein is unlikely to occur because such a process will not deactivate the excited state, unless the BV chromophore deprotonates at some point in the process. Hence, ESPT is the only process that properly explains our experimental observations.[13]

It is interesting to compare the fluorescence properties of phytochromes with those of phycobilisomes, the main light harvesting antenna proteins of cyanobacteria. APC is the best characterized phycobilisome antenna and used as a fluorescence marker.[53] APC trimers bind six PCB chromophores and have a fluorescence quantum yield of 0.68,[53] significantly larger than that of BPh despite binding a very similar chromophore. In APC, the bilin chromophores are tightly bound.[63] Recent NMR studies have demonstrated that in APC, the PCB chromophore has low mobility, whereas in Cph1 and Agp1, the PCB and BV chromophores show a significantly higher mobility.[64] Chromophore mobility generally is considered to provide an important channel for excited-state deactivation in bilin and other extended chromophores: through rotations of single and/or double bonds, excited states may deactivate to the ground state potential energy surface through conical intersections or avoided crossing regions near 90° twist angles.[65–68] In the GFP protein family, chromophore mobility determines whether the protein is bright or dark.[69–71] In the case of BPh, BV twisting may contribute to excited-state decay by inducing ESPT.[13] In addition, BV twisting may directly deactivate the excited state at rates that are comparable to that of ESPT: if the two processes are in competition, H/D exchange may still become apparent in the kinetics because the latter process slows down. Thus, minimizing ESPT processes and constraining the BV chromophore mobility may offer two routes to increasing the BPh fluorescence quantum yield.

Conserved Asp and the PHY domain interaction affect excited-state lifetime and fluorescence quantum yield

Our results show that P3 from *Rps. palustris* has a significantly higher fluorescence quantum yield than classical (bacterio)-phytochromes. In particular the P3 PAS–GAF–PHY D216A mutant shows a level of fluorescence (0.066) that rivals that observed in the engineered IFP4.1 BPh.[30] This observation is quite remarkable given that in P3, just a single amino acid exchange is required to confer these favorable fluorescence properties.

We relate the observed fluorescence quantum yields and excited-state lifetimes in the P3 and P2 variants to the structures available for phytochromes. In the structures, the main-chain carbonyl of this Asp 216 is an integral part of an extensive hydrogen-bonding network with the BV pyrrole nitrogens, a conserved His and a bound water.[24–26,28] In the cyanobacterial Cph1 Pr state crystal structure, the carboxylate side chain of the corresponding conserved Asp-207 doubly hydrogen bonds with Arg-472 from the PRXSF motif of the PHY domain (Fig. 1C).[28] Thus, the conserved Asp connects BV, the GAF domain and the PHY domain. Both the PHY domain and the conserved Asp are required to generate a canonical Pfr or Pnr state[26,27] and for the BV protonation cycle from Meta-R to Pfr.[20,32]

Since there is no structure available for any PAS–GAF–PHY construct of BPh in the Pr state, we base discussion of the interactions between BV and the GAF and PHY domains on the X-ray structure of Cph1[28] (Fig. 1C) in its

Pr state. It should be noted that Cph1 covalently binds a PCB chromophore to its GAF domain rather than a BV chromophore to the PAS domain. Nevertheless, the structures of Cph1 and BPh are sufficiently similar in their PAS and GAF domains[24–26,28] to warrant such a comparison at this stage. In the PaBphP PAS–GAF–PHY crystal structure, the interactions between BV and the PAS–GAF–PHY domains are quite different, but this is very likely due to this structure being in the Pfr state rather than to a fundamental structural difference between BPh and Cph1.[10,28] Comparison with the recently determined cyanobacterial SyB–Cph1 NMR structure is less relevant because SyB–Cph1 lacks any PAS domain (the protein is comprised naturally of GAF–PHY domains) and the structure was that of the isolated GAF domain.[23]

An important observation is that deletion of the PHY domain or replacement of the conserved Asp by Ala in P3 or P2 PAS–GAF–PHY proteins results in a significant increase of the BV excited-state lifetime with respect to their wild type PAS–GAF–PHY constructs. In addition, we observe pronounced H/D exchange effects in all BPh constructs studied. Thus, similar proton transfer events govern excited state dynamics in all these proteins. Because the excited-state lifetime of P3 PAS–GAF and D216A is subject to a KIE of 1.6 and 1.7 respectively, the excited-state lifetime increase of these BPh variants with respect to P3 PAS–GAF–PHY must be a consequence of an ESPT rate decrease upon replacement of Asp with Ala, or upon deletion of the PHY domain.

According to the PAS–GAF–PHY structure of Cph1 in the Pr state, the carboxyl side chain of the conserved Asp forms a double hydrogen bond to a conserved Arg in the PRXSF motif in the PHY domain (Fig. 1C, ref. 28). We assume here that P3 and P2 PAS–GAF–PHY proteins in their Pr states assume a structure in this region similar to that of Cph1 in Pr, as illustrated in Fig. 5A. There, Asp-216 forms a double hydrogen bond with Arg-481 in the P3 PAS–GAF–PHY protein. Obviously, this strong hydrogen bond interaction is absent in the P3 PAS–GAF–PHY D216A and P2 PAS–GAF–PHY D202A mutants. As a consequence, the backbone of the newly inserted Ala may assume a slightly different conformation, which will affect the hydrogen-bond network at the BV pyrrole nitrogens shown in Fig. 1A and B, *i.e.* between BV, the main-chain carbonyl of newly inserted Ala and (possibly) bound water. Similarly, deletion of the PHY domain will eliminate the same hydrogen bonds between the Arg of the PHY domain and the conserved Asp, with the same effect. We propose that the local perturbation of the hydrogen-bond network around the pyrrole nitrogens slows down ESPT. The perturbation may be very small and difficult to observe by X-ray or NMR techniques: an increase in hydrogen-bond length between the BV pyrrole nitrogens and the Asp backbone carbonyl of as little as a few tenths of an Angstrom may be sufficient to produce such an effect.[72] A more definitive molecular picture will have to await detailed structural information on P3 PAS–GAF–PHY, now in progress.

The increase of the BV excited-state lifetime through mutation of the conserved Asp or deletion of the PHY domain obviously affects the fluorescence quantum yield (Fig. 2). Studies are in progress in which both alterations are made: mutate the conserved Asp and delete the PHY domain.

Both Asp and the PHY domain affect high-fluorescent and low-fluorescent Pr conformers in classical BPh

In the P2 PAS–GAF–PHY protein, the BV excited-state dynamics is characterized by two decay components, one 'fast' decay of 43 ps and one 'slow' decay of 170 ps.[13] Both decay components contribute to Lumi-R formation. The fast decay component is dominant with an amplitude 1.5 times greater than that of the slow component. In contrast, P3 PAS–GAF–PHY shows only one long-lived decay component of 330 ps. The occurrence of two distinct decay phases in P2 was assigned to heterogeneity in the Pr ground state, which may result in a distinct excited-state decay rate for each conformer.[13] Such conformational heterogeneity in Pr was reported in DrBphP and Agp1 by resonance Raman spectroscopy,[32,73] for plant Phy and Cph1 by solid-state NMR,[74] and in the Pfr ground state of *Ps. aeruginosa* BPh by crystallography.[10] Note that ground-state heterogeneity is frequently observed in biological photoreceptors[42,75–77] and for the PCB chromophore in solution.[78,79] For application of BPh as a fluorescent probe, it is important to engineer BPh in such a way that it only shows 'slow' excited-state decay components, as such components are associated with a high fluorescence quantum yield.

The P2 PAS–GAF protein also shows excited-state decay with two components, whose lifetimes of 76 and 280 ps are increased in comparison with the PAS–GAF–PHY protein. Importantly, the amplitude of the 'slow' 280 ps component has now become dominant, being 1.5 times greater than that of the fast component (see the DADS in Fig. S1D, ESI†). In the P2 D202A mutant, excited-state decay takes place almost entirely with a single 'slow' time constant of 383 ps (Fig. 4C and S1E, ESI†). Thus, deletion of the PHY domain or replacement of the conserved Asp affects the equilibrium that exists in the Pr ground state between 'fast' and 'slow' reacting Pr conformers. The observation that this equilibrium can be changed and even almost entirely shifted towards the 'slow' conformer by such a minor local structural perturbation strongly suggests that the difference between the conformers finds its origin in the exact configuration of the hydrogen-bond network that connects BV, the conserved Asp and bound water (Fig. 1). The 'fast' and 'slow' reacting Pr conformers may differ in the hydrogen bonding patterns near this site that are apparent in the X-ray structures. In DrBph and Cph1, the BV pyrrole rings hydrogen bond to an internal bound water and to the main-chain carbonyl of the conserved Asp,[24,28] while in P3 the pyrrole rings hydrogen bond only to the main-chain carbonyl of Asp-216[26] (Fig. 1). We propose that the 'fast' reacting conformer corresponds to BV pyrrole hydrogen bonding within a more extensive hydrogen-bond network, while the 'slow' reacting conformer corresponds to BV pyrrole hydrogen bonding only to the Asp backbone carbonyl. This proposal is consistent with the observation of a single slow BV decay component in P3 (Fig. 3 and ref. 13).

The primary photoproducts of P3 PAS–GAF, P3 PAS–GAF–PHY D216A and P2 PAS–GAF–PHY D202A: deprotonated BV states?

In the P2 and P3 PAS–GAF–PHY constructs, Lumi-R is formed with quantum yields of 0.13 and 0.06, respectively.[13] The Lumi-R-minus-Pr difference spectra show a ground state bleach and a red-shifted induced absorption. The latter has an amplitude that is similar to or exceeds that of the bleach, and has a bandwidth comparable to the bleach. Thus, Lumi-R is red-shifted with respect to Pr and has a dipole strength similar to Pr. These features define the spectral properties of canonical Lumi-R. Fig. 6 shows the shapes and relative amplitudes of the BV excited state and the primary photoproduct of P3 PAS–GAF–PHY wild type, P3 PAS–GAF, the P3 PAS–GAF–PHY D216A mutant, P2 PAS–GAF–PHY wild type, P2 PAS–GAF and the P2 PAS–GAF–PHY D202A mutant.

It is difficult to accurately estimate the quantum yield of primary photoproduct formation, as spectrally overlapping contributions by ground-state bleach and photoproduct absorption strongly affect signal amplitude, as does a reduced oscillator strength of the product. Such overlap is least likely to occur for the vibronic bands near 640 nm. By comparing bleach amplitudes of the EADS of BV singlet excited states and photoproducts at this wavelength, one can estimate the yield of the latter.[13] Following this procedure, we arrive at quantum yields of 0.04 (P3 PAS–GAF), 0.03 (P3 D216A), 0.01 (P3 Y272F), 0.10 (P2 PAS–GAF) and 0.09 (P2 D202A) (not shown).

Interestingly, the primary photoproducts of P3 PAS–GAF, P3 PAS–GAF–PHY D216A and P2 PAS–GAF–PHY D202A exhibit difference spectra that deviate substantially from the canonical Lumi-R lineshape observed in the P2 and P3 PAS–GAF–PHY constructs. Hence, their molecular nature must be quite different in these proteins. In particular, the induced absorption of the primary photoproducts has a lower amplitude and is broader overall than in canonical Lumi-R. In addition, the absorption maximum is shifted to the red, to 745 and 755 nm for the P2 D202A and the P3 D216A mutants, respectively. A lower amplitude implies that the dipole strength of the primary photoproduct is significantly reduced with respect to that of canonical Lumi-R. This may be caused by deprotonation of the BV chromophore, such as observed in 'bleached' Meta-R intermediates.[19,21,80] In addition, Meta-R intermediate states have a red-shifted induced absorption relative to Lumi-R states,[19,22,81] possibly arising from a more planar conformation of ring D.[11] Thus, the primary photoproduct in P3 PAS–GAF and the P3 D216A and P2 D202A mutants might resemble the Meta-R intermediate with regard to protonation state and ring D conformation. However, structural relaxation of the protein will not have taken place so the system as a whole is probably still strained. The Meta-R intermediate is normally formed on a much longer timescale (~100 μs) in wild type BPh PAS–GAF–PHY constructs. This observation suggests that the pK_a of BV in its 15*Ea*

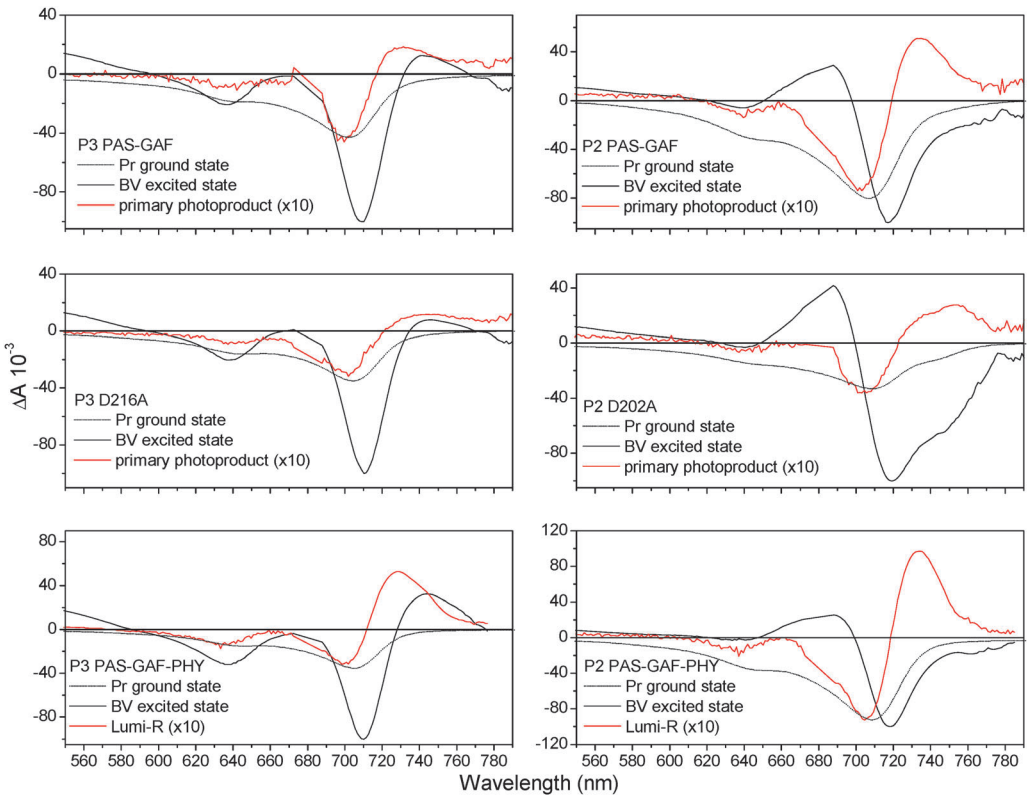

Fig. 6 Comparison of spectral shape and amplitudes of the relaxed BV excited states (black lines) and the primary photoproducts (red lines) for P2 and P3 PAS–GAF, the P3 PAS–GAF–PHY D216A mutant, the P2 PAS–GAF–PHY D202A mutant and P3 and P2 PAS–GAF–PHY. The dashed lines indicate the Pr ground-state absorption profiles.

configuration is significantly affected by the amino acid identity at position 216 (P3 numbering), as shown earlier for Agrobacterium Agp1 phytochrome.[20]

Abbreviations

BPh	bacteriophytochrome
BV	biliverdin
PCB	phycocyanobilin
PΦB	phycochromobilin
KIE	kinetic isotope effect
EADS	evolution-associated difference spectrum
DADS	decay-associated difference spectrum
DAS	decay-associated spectrum
ESPT	excited-state proton transfer
APC	allophycocyanine

Acknowledgements

K.C.T. and J.T.M.K. were supported by the Earth and Life Sciences Council of the Netherlands Foundation for Scientific Research (NWO-ALW) through a VIDI grant to J.T.M.K. E.A.S and K.M. were supported by NIH grant GM036452 to K.M.

References

1 H. A. Borthwick, S. B. Hendricks, M. W. Parker, E. H. Toole and V. K. Toole, *Proc. Natl. Acad. Sci. U. S. A.*, 1952, **38**, 662–666.
2 W. L. Butler, K. H. Norris, H. W. Siegelman and S. B. Hendricks, *Proc. Natl. Acad. Sci. U. S. A.*, 1959, **45**, 1703–1708.
3 S. J. Davis, A. V. Vener and R. D. Vierstra, *Science*, 1999, **286**, 2517–2520.
4 J. Hughes, T. Lamparter, F. Mittmann, E. Hartmann, W. Gartner, A. Wilde and T. Borner, *Nature*, 1997, **386**, 663.
5 T. Lamparter, N. Michael, F. Mittmann and B. Esteban, *Proc. Natl. Acad. Sci. U. S. A.*, 2002, **99**, 11628–11633.
6 A. Blumenstein, K. Vienken, R. Tasler, J. Purschwitz, D. Veith, N. Frankenberg-Dinkel and R. Fischer, *Curr. Biol.*, 2005, **15**, 1833–1838.
7 N. C. Rockwell, Y. S. Su and J. C. Lagarias, *Annu. Rev. Plant Biol.*, 2006, **57**, 837–858.
8 M. E. Auldridge and K. T. Forest, *Crit. Rev. Biochem. Mol. Biol.*, 2011, **46**, 67–88.
9 H. Li, J. R. Zhang, R. D. Vierstra and H. L. Li, *Proc. Natl. Acad. Sci. U. S. A.*, 2010, **107**, 10872–10877.
10 X. Yang, J. Kuk and K. Moffat, *Proc. Natl. Acad. Sci. U. S. A.*, 2008, **105**, 14715–14720.
11 T. Rohmer, C. Lang, J. Hughes, L. O. Essen, W. Gartner and J. Matysik, *Proc. Natl. Acad. Sci. U. S. A.*, 2008, **105**, 15229–15234.
12 M. A. Mroginski, D. H. Murgida and P. Hildebrandt, *Acc. Chem. Res.*, 2007, **40**, 258–266.
13 K. C. Toh, E. A. Stojkovic, I. H. M. van Stokkum, K. Moffat and J. T. M. Kennis, *Proc. Natl. Acad. Sci. U. S. A.*, 2010, **107**, 9170–9175.
14 J. J. van Thor, K. L. Ronayne and M. Towrie, *J. Am. Chem. Soc.*, 2007, **129**, 126–132.
15 C. Schumann, R. Gross, N. Michael, T. Lamparter and R. Diller, *ChemPhysChem*, 2007, **8**, 1657–1663.
16 K. Heyne, J. Herbst, D. Stehlik, B. Esteban, T. Lamparter, J. Hughes and R. Diller, *Biophys. J.*, 2002, **82**, 1004–1016.
17 F. Andel, K. C. Hasson, F. Gai, P. A. Anfinrud and R. A. Mathies, *Biospectroscopy*, 1997, **3**, 421–433.
18 M. G. Muller, I. Lindner, I. Martin, W. Gartner and A. R. Holzwarth, *Biophys. J.*, 2008, **94**, 4370–4382.
19 B. Borucki, D. von Stetten, S. Seibeck, T. Lamparter, N. Michael, M. A. Mroginski, H. Otto, D. H. Murgida, M. P. Heyn and P. Hildebrandt, *J. Biol. Chem.*, 2005, **280**, 34358–34364.
20 D. von Stetten, S. Seibeck, N. Michael, P. Scheerer, M. A. Mroginski, D. H. Murgida, N. Krauss, M. P. Heyn, P. Hildebrandt, B. Borucki and T. Lamparter, *J. Biol. Chem.*, 2007, **282**, 2116–2123.
21 P. Piwowarski, E. Ritter, K. P. Hofmann, P. Hildebrandt, D. von Stetten, P. Scheerer, N. Michael, T. Lamparter and F. Bartl, *ChemPhysChem*, 2010, **11**, 1207–1214.
22 E. Giraud, S. Zappa, L. Vuillet, J. M. Adriano, L. Hannibal, J. Fardoux, C. Berthomieu, P. Bouyer, D. Pignol and A. Vermeglio, *J. Biol. Chem.*, 2005, **280**, 32389–32397.
23 A. T. Ulijasz, G. Cornilescu, C. C. Cornilescu, J. R. Zhang, M. Rivera, J. L. Markley and R. D. Vierstra, *Nature*, 2010, **463**, 250–U143.
24 J. R. Wagner, J. S. Brunzelle, K. T. Forest and R. D. Vierstra, *Nature*, 2005, **438**, 325–331.
25 J. R. Wagner, J. Zhang, J. S. Brunzelle, R. D. Vierstra and K. T. Forest, *J. Biol. Chem.*, 2007, **282**, 12298–12309.
26 X. Yang, E. A. Stojkovic, J. Kuk and K. Moffat, *Proc. Natl. Acad. Sci. U. S. A.*, 2007, **104**, 12571–12576.
27 J. R. Wagner, J. Zhang, D. von Stetten, M. Gunther, D. H. Murgida, M. A. Mroginski, J. M. Walker, K. T. Forest, P. Hildebrandt and R. D. Vierstra, *J. Biol. Chem.*, 2008, **283**, 12212–12226.
28 L. O. Essen, J. Mailliet and J. Hughes, *Proc. Natl. Acad. Sci. U. S. A.*, 2008, **105**, 14709–14714.
29 Y. Oka, T. Matsushita, N. Mochizuki, T. Suzuki, S. Tokutomi and A. Nagatani, *Plant Cell*, 2004, **16**, 2104–2116.
30 X. Shu, A. Royant, M. Z. Lin, T. A. Aguilera, V. Lev-Ram, P. A. Steinbach and R. Y. Tsien, *Science*, 2009, **324**, 804–807.
31 A. J. Fischer and J. C. Lagarias, *Proc. Natl. Acad. Sci. U. S. A.*, 2004, **101**, 17334–17339.
32 J. R. Wagner, J. R. Zhang, D. von Stetten, M. Guenther, D. H. Murgida, M. A. Mroginski, J. M. Walker, K. T. Forest, P. Hildebrandt and R. D. Vierstra, *J. Biol. Chem.*, 2008, **283**, 12212–12226.
33 J. A. Zhang, X. J. Wu, Z. B. Wang, Y. Chen, X. Wang, M. Zhou, H. Scheer and K. H. Zhao, *Angew. Chem., Int. Ed.*, 2010, **49**, 5456–5458.
34 K. C. Toh, E. A. Stojkovic, A. B. Rupenyan, I. H. M. van Stokkum, M. Salumbides, M. L. Groot, K. Moffat and J. T. M. Kennis, *J. Phys. Chem. A*, 2011, **115**, 3778–3786.
35 R. Berera, R. van Grondelle and J. T. M. Kennis, *Photosynth. Res.*, 2009, **101**, 105–118.
36 B. Gobets, I. H. M. van Stokkum, M. Rogner, J. Kruip, E. Schlodder, N. V. Karapetyan, J. P. Dekker and R. van Grondelle, *Biophys. J.*, 2001, **81**, 407–424.
37 B. Gobets, J. T. M. Kennis, J. A. Ihalainen, M. Brazzoli, R. Croce, L. H. M. van Stokkum, R. Bassi, J. P. Dekker, H. van Amerongen, G. R. Fleming and R. van Grondelle, *J. Phys. Chem. B*, 2001, **105**, 10132–10139.
38 I. H. M. van Stokkum, D. S. Larsen and R. van Grondelle, *Biochim. Biophys. Acta, Bioenerg.*, 2004, **1657**, 82–104.
39 J. T. M. Kennis and M. L. Groot, *Curr. Opin. Struct. Biol.*, 2007, **17**, 623–630.
40 E. Papagiannakis, J. T. M. Kennis, I. H. M. van Stokkum, R. J. Cogdell and R. van Grondelle, *Proc. Natl. Acad. Sci. U. S. A.*, 2002, **99**, 6017–6022.
41 C. Bonetti, M. T. A. Alexandre, I. H. M. van Stokkum, R. G. Hiller, M. L. Groot, R. van Grondelle and J. T. M. Kennis, *Phys. Chem. Chem. Phys.*, 2010, **12**, 9256–9266.
42 R. Berera, I. H. M. van Stokkum, G. Kodis, A. E. Keirstead, S. Pillai, C. Herrero, R. E. Palacios, M. Vengris, R. van Grondelle, D. Gust, T. A. Moore, A. L. Moore and J. T. M. Kennis, *J. Phys. Chem. B*, 2007, **111**, 6868–6877.
43 C. C. Gradinaru, J. T. M. Kennis, E. Papagiannakis, I. H. M. van Stokkum, R. J. Cogdell, G. R. Fleming, R. A. Niederman and R. van Grondelle, *Proc. Natl. Acad. Sci. U. S. A.*, 2001, **98**, 2364–2369.
44 C. Bonetti, T. Mathes, I. H. M. van Stokkum, K. M. Mullen, M. L. Groot, R. van Grondelle, P. Hegemann and J. T. M. Kennis, *Biophys. J.*, 2008, **95**, 4790–4802.

45 R. B. Mujumdar, L. A. Ernst, S. R. Mujumdar, C. J. Lewis and A. S. Waggoner, *Bioconjugate Chem.*, 1993, **4**, 105–111.
46 J. R. Lakowicz, *The principles of fluorescence spectroscopy*, Springer.
47 W. S. Struve, *Biophys. J.*, 1995, **69**, 2739–2744.
48 J. Dasgupta, R. R. Frontiera, K. C. Taylor, J. C. Lagarias and R. A. Mathies, *Proc. Natl. Acad. Sci. U. S. A.*, 2009, **106**, 1784–1789.
49 A. Wilson, C. Punginelli, A. Gall, C. Bonetti, M. Alexandre, J. M. Routaboul, C. A. Kerfeld, R. van Grondelle, B. Robert, J. T. M. Kennis and D. Kirilovsky, *Proc. Natl. Acad. Sci. U. S. A.*, 2008, **105**, 12075–12080.
50 J. Wendler, A. R. Holzwarth, S. E. Braslavsky and K. Schaffner, *Biochim. Biophys. Acta*, 1984, **786**, 213–221.
51 P. S. Song, Q. Chae and J. D. Gardner, *Biochim. Biophys. Acta*, 1979, **576**, 479–495.
52 J. C. Litts, J. M. Kelly and J. C. Lagarias, *J. Biol. Chem.*, 1983, **258**, 1025–1031.
53 A. N. Glazer, *J. Appl. Phycol.*, 1994, **6**, 105–112.
54 G. F. W. Searle, J. Barber, G. Porter and C. J. Tredwell, *Biochim. Biophys. Acta*, 1978, **501**, 246–256.
55 A. M. Kuznetsov and J. Ulstrup, *Can. J. Chem.*, 1999, **77**, 1085–1096.
56 H. M. Strauss, J. Hughes and P. Schmieder, *Biochemistry*, 2005, **44**, 8244–8250.
57 C. Kneip, P. Hildebrandt, W. Schlamann, S. E. Braslavsky, F. Mark and K. Schaffner, *Biochemistry*, 1999, **38**, 15185–15192.
58 O. A. Borg and B. Durbeej, *J. Phys. Chem. B*, 2007, **111**, 11554–11565.
59 H. Falk, K. Grubmayr and F. Neufingerl, *Monatsh. Chem.*, 1977, **108**, 1185–1188.
60 A. H. Goller, D. Strehlow and G. Hermann, *ChemPhysChem*, 2005, **6**, 1259–1268.
61 B. Zienicke, L. Y. Chen, H. Khawn, M. A. S. Hammam, H. Kinoshita, J. Reichert, A. S. Ulrich, K. Inomata and T. Lamparter, *J. Biol. Chem.*, 2011, **286**, 1103–1113.
62 A. A. Samma, C. K. Johnson, S. A. Song, S. Alvarez and M. Zimmer, *J. Phys. Chem. B*, 2010, **114**, 15362–15369.
63 K. Brejc, R. Ficner, R. Huber and S. Steinbacher, *J. Mol. Biol.*, 1995, **249**, 424–440.
64 M. Roben, J. Hahn, E. Klein, T. Lamparter, G. Psakis, J. Hughes and P. Schmieder, *ChemPhysChem*, 2010, **11**, 1248–1257.
65 P. Altoe, T. Climent, G. C. De Fusco, M. Stenta, A. Bottoni, L. Serrano-Andres, M. Merchan, G. Orlandi and M. Garavelli, *J. Phys. Chem. B*, 2009, **113**, 15067–15073.
66 R. Gonzalez-Luque, M. Garavelli, F. Bernardi, M. Merchan, M. A. Robb and M. Olivucci, *Proc. Natl. Acad. Sci. U. S. A.*, 2000, **97**, 9379–9384.
67 M. Ben-Nun, F. Molnar, K. Schulten and T. J. Martinez, *Proc. Natl. Acad. Sci. U. S. A.*, 2002, **99**, 1769–1773.
68 W. Humphrey, H. Lu, I. Logunov, H. J. Werner and K. Schulten, *Biophys. J.*, 1998, **75**, 1689–1699.
69 H. Mizuno, T. K. Mal, M. Walchli, A. Kikuchi, T. Fukano, R. Ando, J. Jeyakanthan, J. Taka, Y. Shiro, M. Ikura and A. Miyawaki, *Proc. Natl. Acad. Sci. U. S. A.*, 2008, **105**, 9227–9232.
70 D. Mandal, T. Tahara and S. R. Meech, *J. Phys. Chem. B*, 2004, **108**, 1102–1108.
71 M. Vengris, I. H. M. van Stokkum, X. He, A. F. Bell, P. J. Tonge, R. van Grondelle and D. S. Larsen, *J. Phys. Chem. A*, 2004, **108**, 4587–4598.
72 S. Scheiner, *Acc. Chem. Res.*, 1985, **18**, 174–180.
73 D. von Stetten, M. Gunther, P. Scheerer, D. H. Murgida, M. A. Mroginski, N. Krauss, T. Lamparter, J. Zhang, D. M. Anstrom, R. D. Vierstra, K. T. Forest and P. Hildebrandt, *Angew. Chem., Int. Ed.*, 2008, **47**, 4753–4755.
74 C. Song, G. Psakis, C. Lang, J. Mailliet, W. Gartner, J. Hughes and J. Matysik, *Proc. Natl. Acad. Sci. U. S. A.*, 2011, **108**, 3842–3847.
75 D. S. Larsen, I. H. M. van Stokkum, M. Vengris, M. A. van der Horst, F. L. de Weerd, K. J. Hellingwerf and R. van Grondelle, *Biophys. J.*, 2004, **87**, 1858–1872.
76 M. Gauden, J. S. Grinstead, W. Laan, H. M. van Stokkum, M. Avila-Perez, K. C. Toh, R. Boelens, R. Kaptein, R. van Grondelle, K. J. Hellingwerf and J. T. M. Kennis, *Biochemistry*, 2007, **46**, 7405–7415.
77 J. S. Grinstead, S. T. D. Hsu, W. Laan, A. Bonvin, K. J. Hellingwerf, R. Boelens and R. Kaptein, *ChemBioChem*, 2006, **7**, 187–193.
78 B. Dietzek, R. Maksimenka, G. Hermann, W. Kiefer, J. Popp and M. Schmitt, *ChemPhysChem*, 2004, **5**, 1171–1177.
79 M. Schmitt, B. Dietzek, G. Hermann and J. Popp, *Laser Photonics Rev.*, 2007, **1**, 57–78.
80 D. von Stetten, S. Seibeck, N. Michael, P. Scheerer, M. A. Mroginski, D. H. Murgida, N. Krauss, M. P. Heyn, P. Hildebrandt, B. Borucki and T. Lamparter, *J. Biol. Chem.*, 2007, **282**, 2116–2123.
81 C. F. Zhang, D. L. Farrens, S. C. Björling, P. S. Song and D. S. Kliger, *J. Am. Chem. Soc.*, 1992, **114**, 4569.

Electronic Supplementary Material (ESI) for Physical Chemistry Chemical Physics

Supporting Information to

Fluorescence quantum yield and photochemistry of bacteriophytochrome constructs

K.C. Toh, Emina A. Stojković, Ivo H.M. van Stokkum, Keith Moffat, John T.M Kennis

Model based data analysis

The aim of data analysis is to obtain a model-based description of the full data set in terms of a model containing a small number of precisely estimated parameters, of which the rate constants and spectra are the most relevant. The basic ingredient of kinetic models, namely the exponential decays, will be described first, followed by use of these ingredients for global and target analysis[1-3] of the full data. Our main assumption is that the time and wavelength properties of the system of interest are separable, which means that spectra of species or states are constant. For details on parameter estimation techniques the reader is referred to[1-4]. Software issues are discussed in[5].

A. Modeling an exponential decay

Here an expression is derived for describing an exponentially decaying component. The instrument response function (IRF) *i(t)* can usually adequately be modeled with a Gaussian with parameters μ and Δ for, respectively, location and full width at half maximum (FWHM):

$$i(t) = \frac{1}{\tilde{\Delta}\sqrt{2\pi}} \exp(-\log(2)(2(t-\mu)/\Delta)^2)$$

where $\tilde{\Delta} = \Delta/(2\sqrt{2\log(2)})$. The convolution (indicated by an *) of this IRF with an exponential decay (with rate *k*) yields an analytical expression which facilitates the estimation of the IRF parameters μ and Δ:

$$c^1(t,k,\mu,\Delta) = \exp(-kt) * i(t) = \frac{1}{2}\exp(-kt)\exp(k(\mu + \frac{k\tilde{\Delta}^2}{2}))\{1 + erf(\frac{t-(\mu+k\tilde{\Delta}^2)}{\sqrt{2}\tilde{\Delta}}\}$$

The wavelength dependence of the IRF location μ can be modeled with a polynomial.

$$\mu(\lambda) = \mu_{\lambda_c} + \sum_{j=1}^{j_{\max}} a_j (\lambda - \lambda_c)^j$$

Typically, a parabola is adequate and the order of this polynomial ($j_{\max}$) is two. The reference wavelength λ_c is usually at the center of the spectrograph.

B. Global and target analysis

The basis of global analysis is the superposition principle, which states that the measured data $\psi(t,\lambda)$ result from a superposition of the spectral properties $\varepsilon_l(\lambda)$ of the components present in the system of interest weighted by their concentration $c_l(t)$.

$$\psi(t,\lambda) = \sum_{l=1}^{n_{comp}} c_l(t)\varepsilon_l(\lambda)$$

The $c_l(t)$ of all n_{comp} components are described by a compartmental model that consists of first-order differential equations, with as solution sums of exponential decays. We consider three types of compartmental models: (1) a model with components decaying monoexponentially in parallel, which yields Decay Associated Difference Spectra (DADS), (2) a sequential model with increasing lifetimes, also called an unbranched unidirectional model[6], which yields Evolution Associated Difference Spectra (EADS), and (3) a full compartmental scheme which may include possible branchings and equilibria, which yields Species Associated Difference Spectra (SADS). The last is most often referred to as target analysis, where the target is the proposed kinetic scheme, including possible spectral assumptions. In this paper we did not attempt a target analysis. Instead, throughout the manuscript, the EADS are shown in the main text and the corresponding DADS are shown in the Supporting Information.

(1) With parallel decaying components the model reads

$$\psi(t,\lambda) = \sum_{l=1}^{n_{comp}} c^I(k_l) DADS_l(\lambda)$$

The DADS thus represent the estimated amplitudes of the above defined exponential decays $c^I(k_l)$. When the system consists of parallel decaying components the DADS are true species difference spectra. In all other cases, they are interpreted as a weighted sum (with both positive and negative contributions) of true species difference spectra.

(2) A sequential model reads

$$\psi(t,\lambda) = \sum_{l=1}^{n_{comp}} c_l^{II} EADS_l(\lambda)$$

where each concentration is a linear combination of the exponential decays,

$c_l^{II} = \sum_{j=1}^{l} b_{jl} c^I(k_l)$, and the amplitudes[6] b_{jl} are given by $b_{11} = 1$ and for $j \le l$:

$$b_{jl} = \prod_{m=1}^{l-1} k_m \Big/ \prod_{n=1, n\neq j}^{l} (k_n - k_j)$$

When the system consists of sequentially decaying components $1 \to 2 \to \ldots \to n_{comp}$ the EADS are true species difference spectra. In all other cases, they are interpreted as a weighted sum (with only positive contributions) of true species difference spectra.

Equivalence of the parallel and the sequential model

It is important to note that the fit is identical when using a parallel or a sequential model. Both the estimated lifetimes and the residuals from the fit are identical. This can be demonstrated as follows. Since the concentrations of the sequential model are a linear combination of the exponential decays we can write for the matrix of concentrations (where column *l* corresponds to component *l*)

$$C^{II} = C^I B$$

where the upper triangular matrix B contains the elements b_{jl} defined above. Furthermore, in matrix notation the parallel model reads

$$\Psi = C^I DADS^T$$

where $DADS^T$ is the transpose of the matrix that contains the DADS of component *l* in column *l*. Likewise, in matrix notation the sequential model reads

$$\Psi = C^{II} EADS^T$$

Combining these three equations we obtain the relations

$$DADS = EADS \cdot B^T$$

$$EADS = DADS \cdot B^{-T}$$

where the coefficients of the lower triangular matrix B^{-T} are given by $b_{1l}^{-1} = 1 = b_{1l}^{-T}$ and for $j \le l$:

$$b_{jl}^{-1} = \prod_{n=1}^{j-1} \frac{(k_n - k_l)}{k_n} = b_{lj}^{-T}$$

Thus the DADS are linear combinations of the EADS, and vice versa. Thus, the *l*th EADS is a linear combination of the *l*th and following DADS. In particular, the first EADS, which corresponds to the time zero difference spectrum, is the sum of all DADS; and the final EADS is proportional to the final DADS.

In systems where photophysical and photochemical processes occur the sequential model with increasing lifetimes provides a convenient way to visualize the evolution of the (excited and intermediate) states of the system. Therefore, the EADS are shown in the main text and the corresponding DADS are shown in the Supporting Information.

References

(1) Holzwarth, A. R. Data Analysis of Time-Resolved Measurements. In *Biophysical Techniques in Photosynthesis*; Amesz, J., Hoff, A. J., Eds.; Kluwer: Dordrecht, The Netherlands, 1996; pp 75.

(2) van Stokkum, I. H. M.; Larsen, D. S.; van Grondelle, R. *Biochimica Et Biophysica Acta-Bioenergetics* **2004**, *1657*, 82.

(3) van Stokkum, I. H. M.; van Oort, B.; van Mourik, F.; Gobets, B.; van Amerongen, H. (Sub)-Picosecond Spectral Evolution of Fluorescence Studied with a Synchroscan Streak-Camera System and Target Analysis. In *Biophysical Techniques in Photosynthesis Vol. II*; Aartsma, T. J., Matysik, J., Eds.; Springer: Dordrecht, The Netherlands, 2008; pp 223.

(4) van Stokkum, I. H. M. "Global and Target Analysis of Time-resolved Spectra," Department of Physics and Astronomy, Faculty of Sciences, Vrije Universiteit, Amsterdam, The Netherlands, 2005.

(5) van Stokkum, I. H. M.; Bal, H. E. "A Problem Solving Environment for interactive modelling of multiway data", 2006.

(6) Nagle, J. F.; Parodi, L. A.; Lozier, R. H. *Biophysical Journal* **1982**, *38*, 161.